



Integrated Computational Materials Engineering to Predict Dimensions for Steady-State and Transient Melt-Pool Formation in the Selective Laser Melting of Inconel 625

Stephen Wormald¹ · Jordan Clingenpeel¹ · Tim Vincent¹ · Anil Chaudhary¹

Received: 12 March 2021 / Accepted: 3 July 2021 / Published online: 15 July 2021
© The Minerals, Metals & Materials Society 2021

Abstract

This work presents solutions to Challenge 2 within the Air Force Research Laboratory Materials Inform Data-Driven Design for AM Structures (MID3AS) AM (Additive Manufacturing) Challenge. The solutions are for quasi-steady-state and transient N th-track cross-sectional predictions as a function of scan paths. Tracks are deposited successively to produce a pad and overlap each other; their cross section is defined using four dimensions: total depth, remelt depth, half width, and width increment due to the addition of the latest (N th) track. There are six pads for which the pad dimensions, build height, power, scan speed, hatch spacing, and number of tracks are varied. There also are two thin walls that consist of 10 single tracks deposited on top of each other. The track cross sections are to be reported at three measurement planes defined orthogonal to the scan path at varying distances from the start of a track in the quasi-steady-state and transient melt-pool regions. The predictions are generated using the Additive Manufacturing Parameter Predictor (AMP²) software that performed multi-scale simulations for the six pads and two thin walls. Two types of melt-pool simulations were performed: a quasi-steady-state, thermal-computational fluid dynamics simulation and a transient thermal simulation. The statistics of track dimensions were estimated using discrete element modeling to predict the local variation in recoat powder density and correcting for the additive mass consolidated by a track cross section accordingly. Applied Optimization, Inc. achieved third place for the accuracy of predictions required by Challenge 2 in the MID3AS AM Challenge.

Keywords Inconel 625 · Melt-pool model · Track cross-sectional prediction · Remelt depth · Effect of scan path · Track-on-track

Introduction

Additive manufacturing (AM) promises to enable an increased degree of freedom when designing complex part geometries with enhanced material properties. For the laser powder bed fusion (LPBF) process, a part is built from thousands to millions of individual track vectors. As the laser moves along a track vector, a melt pool forms that may change in shape and size depending on position and local temperature, which in turn can influence microstructure inhomogeneity, the prevalence of porosity, and resulting

macroscopic material properties. If process models can predict key elements of transient melt-pool formation, they may be used to tune LPBF parameters, optimize AM processes, and maximize part quality.

Existing, off-the-shelf, AM simulation software may be evaluated through blind assessment in modeling challenges. The Air Force Research Laboratory (AFRL) launched an AM modeling challenge series Materials Inform Data-Driven Design for Additive Structures (MID3AS) AM Challenge (or MID3AS AM Challenge for short) in 2018, where the second challenge problem (Challenge 2) addressed microscale process-to-structure predictions [1–4]. The challenge asked contestants to predict melt-pool cross-sectional dimensions, where the process varied from quasi-steady-state to transient.

✉ Anil Chaudhary
anil@appliedo.com

¹ Applied Optimization, Inc., 3040 Presidential Dr. Suite 100,
Fairborn, OH 45324, USA

This paper describes an entry submitted by Applied Optimization, Inc. (AO) for Challenge 2, where we used off-the-shelf version of the AM Parameter Predictor (AMP²) software suite developed by AO to perform the predictions and achieve third place in the challenge. Prior to the MID3AS AM Challenge, AMP² results received second place in the DARPA modeling challenge in 2017 and the NIST AM Benchmark Test Series problem AMB2018-02 [5, 6]. The DARPA challenge objective was to evaluate the accuracy of simulating the thermal and microstructural response of alloy Inconel 718 (IN718) a material during the laser powder bed AM process. The NIST AMB2018-02 objective was to predict the solidification grain structure and orientation for a series of single-scan tracks on a bare metal substrate of alloy Inconel 625 (IN625).

Analysis

AFRL Challenge Statement

The AFRL statement for Challenge 2 was issued in order to assess the participants’ ability to model and predict the dimensions and variability of solidified melt-pool cross sections. Eight sets of LPBF tracks were produced using

the IN625 alloy, where the build plate was plain carbon steel. Each of the eight challenge items was deposited on a 5-mm-thick AM pad of IN625. All pads were rectangular in shape and extended beyond the bounding box of the corresponding challenge item by at least 3 mm. Six of the challenge items were single layers, while two were 10-layer high, single-track thin walls. Figure 1 shows the IDs, size, number of tracks, and process parameters for each of the challenge items. Challenge items B21 and B25 are 10-layer high, single-track thick walls, while items B26–B38 are pads of consecutive track vectors.

Participants were asked to measure the track cross sections along “measurement planes” which were perpendicular to the track direction. Table 1 shows the location of the measurement planes on the *x*-coordinate (along the length) for each challenge item. An “N/A” represents the absence of a measurement plane. Each measurement plane is indicated by the dotted lines in Fig. 1. Note that measurement planes closer to the end of the track vectors were expected to experience transient melt-pool formation due to variable temperatures caused by the laser turnaround, compared to the center measurement planes where the temperature between tracks was expected to be more uniform. The AMP² software suite was used to predict track dimensions for each measurement plane. Section 2.2 describes the AM modeling procedure

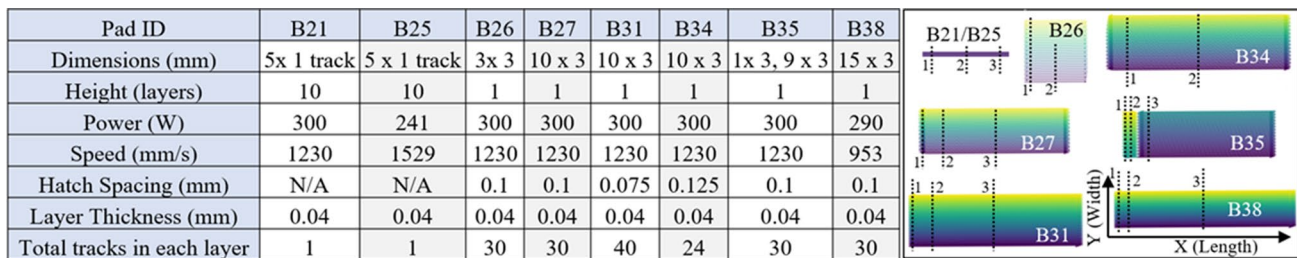


Fig. 1 Track sets deposited for the MID3AS AM Challenge. Parameters and track definitions are provided where the deposit type varies between track-on-track deposits (samples B21 and B25) and pads of multiple tracks. The track pads vary in length and number of tracks,

as shown in rightmost image. The blue lines were deposited before the yellow lines. The black-dotted lines and numbers correspond to the measurement planes in Table 1

Table 1 Measurement plane locations and AMP² model type used to predict the corresponding melt-pool dimensions

Pad ID	Measurement plane 1		Measurement plane 2		Measurement plane 3	
	Location (mm)	Model type	Location (mm)	Model type	Location (mm)	Model type
B21	0.25	Quasi-steady thermal-CFD	2.5	Quasi-steady thermal-CFD	4.75	Quasi-steady thermal-CFD
B25	0.25	Quasi-steady thermal-CFD	2.5	Quasi-steady thermal-CFD	4.75	Quasi-steady thermal-CFD
B26	0.1	Transient thermal	1.5	Quasi-steady thermal-CFD	N/A	N/A
B27	0.1	Transient thermal	1.5	Quasi-steady thermal-CFD	5	Quasi-steady thermal-CFD
B31	0.1	Transient thermal	1.5	Quasi-steady thermal-CFD	5	Quasi-steady thermal-CFD
B34	1.5	Quasi-steady thermal-CFD	5	Quasi-steady thermal-CFD	N/A	N/A
B35	0.1	Transient thermal	0.5	Transient thermal	1.5	Quasi-steady thermal-CFD
B38	0.1	Transient thermal	1.5	Quasi-steady thermal-CFD	7.5	Quasi-steady thermal-CFD

used by AMP². The simulation type differed depending on whether a measurement plane would experience transient or steady-state melt-pool formation. The choice to perform transient and semi-steady-state simulation was based on the temperature predictions given by the layer-scale simulation (Sect. 2.2). A second, salient reason was the choice made by AO to limit the submission of results to only those produced by the algorithms presently available in the off-the-shelf, commercial version of AMP² software suite to provide a blind assessment of results that can be independently reproduced by a 3rd party user.

AMP² Process Model and Simulation Approach

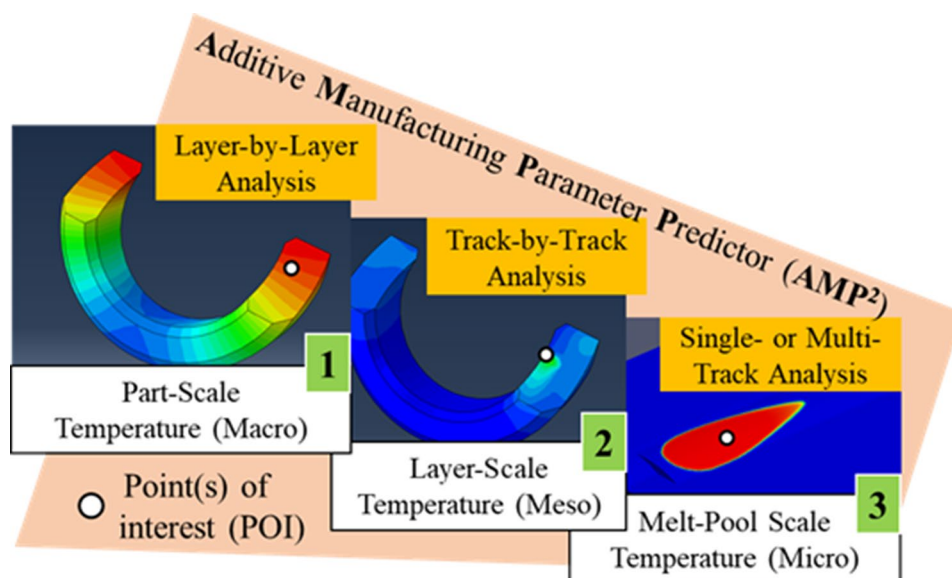
When modeling the LPBF process, the local powder distribution, local geometry of deposited material, geometry of adjacent tracks, local temperature distribution, and other factors influence the formation of individual melt pools. A challenge in modeling these factors is that the current track is affected, thermally and geometrically, by all previously deposited tracks. As modeling each track at the microscale (melt-pool scale) is often too time intensive, multi-scale process models may simulate a Point of Interest (POI) to glean valuable insight and improve an AM process.

The Additive Manufacturing Parameter Predictor (AMP²) is an Integrated Computational Materials Engineering (ICME) software suite to predict Feature Specific Parameters (FSP) for the AM of high-quality, net-shape, as-built material based on the predictions of multi-scale, multi-physics simulations [7–11]. AMP² was created by AO through the maintenance, integration, and commercialization efforts after NAVAIR, NASA, and ONR Small Business Innovative Research (SBIR) programs. AMP² models the LPBF process at the macroscale (part scale,

layer-by-layer analysis), mesoscale (layer-scale, track-by-track analysis), and microscale (melt-pool scale, single or multi-track analysis). A quasi-steady-state, melt-pool simulation is performed using the microscale model, which performs thermal-computational fluid dynamics (CFD) simulations. A transient melt-pool simulation is performed using the mesoscale model, which performs transient thermal simulations. Both types of melt-pool simulations account for phase change. Each reduced simulation scale is initialized using thermal boundary conditions from the larger scale, thereby preserving the influence of depositing prior tracks. Figure 2 shows a flowchart of the AMP² simulation process.

The microscale, quasi-steady-state, melt-pool, thermal-CFD model uses an iterative geometry model to simulate the melt-pool shape, temperature, and fluid flow [6]. Since the melt-pool dimensions are unknown a priori, the size of the microscale model domain is set automatically by its iterative solution, which computes the melt-pool dimensions. The thermal boundary conditions for the melt-pool simulation at a given location are generated from the macroscale and mesoscale simulations. Although the temperature distribution at the part and layer scale is nonuniform, the thermal boundary conditions for the melt-pool simulation are assumed to be steady-state, corresponding to the temperature distribution on a plane perpendicular to the longitudinal axis of the laser track at the location of interest. In Fig. 2, such a plane would be a radial cross section through the wall of the part. Accordingly, the melt-pool thermal-CFD simulations solve the incompressible Navier–Stokes equations and the thermal energy equation with a solid–liquid phase change for steady-state melt-pool formation. From the numerical analysis, the melt-pool geometry, flow field, and temperature distribution

Fig. 2 AMP² multi-scale, multi-physics process model



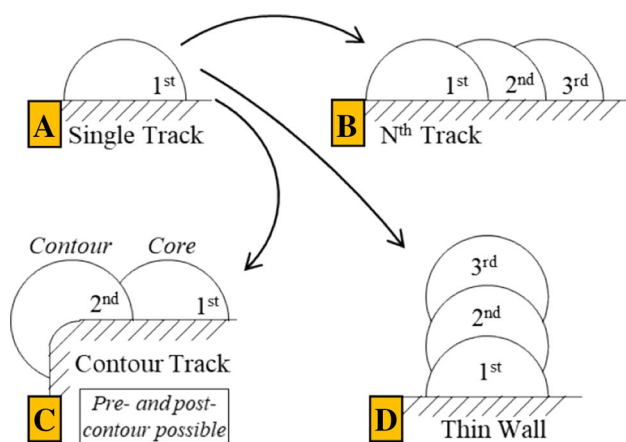


Fig. 3 Thermal-CFD melt-pool prediction, showing representative cross sections for a **a** single track, **b** N th track, **c** contour track, and **d** thin wall simulation. Simulation types B–D may be initialized using the single-track geometry

are predicted. The melt-pool cross-sectional geometry and length are computed iteratively such that the thermal and fluid flow equilibrium conditions are fulfilled.

Four types of quasi-steady-state, melt-pool, thermal-CFD simulations may be run, as shown in Fig. 3: (1) single track, (2) multi-track (or N th-track), (3) contour tracks, and (4) track-on-track deposits. Each of these thermal-CFD simulations accounts for the substrate shape and the powder mass consumed by the melt pool due to the formation of the powder denudation zone (PDZ) around its periphery (i.e., adjacent to one or both sides and the front end of a track). The PDZ width is estimated to equal the mean powder radius. The substrate shape accounts for the cross-sectional geometry of the preceding layer and the preceding track. A single-track simulation models track formation on virgin powder (i.e., 1st track on powder recoat, Fig. 3a). A simulation for N th-track models track formation when the preceding $N - 1$ tracks have been deposited (e.g., Fig. 3b when $N = 3$). A contour track is deposited around the circumference of a layer (Fig. 3c). Contour tracks can be pre- or post-contour, depending on the order in which the core tracks and contour track are deposited. For pre-contour, the contour track is deposited first, followed by the core tracks. For post-contour, the core tracks are deposited first, followed by the contour track. For track-on-track deposits, the shape of preceding layer is the top surface of the preceding single track (Fig. 3d). Note the quasi-steady thermal-CFD in Table 1 are N th-track simulations as these represent the experiment.

However, the thermal-CFD melt-pool model assumes steady-state melt-pool formation. While this approximation may be meaningful for quasi-steady-state situations, the melt-pool geometry may vary more significantly in highly transient regions. The AMP² mesoscale transient thermal simulation was therefore used to approximate the prediction

of transient melt-pool formation at a microscale. The laser heat source moves incrementally within the single track as it crosses the measurement plan, along the predefined scan path, where the scan path was generated as specified by the AFRL challenge statement. Mesh size and time step of the mesoscale simulation was automatically refined to provide transient temperature prediction at a microscale. For the quasi-steady-state thermal-CFD simulations, the mesh is refined to a level fine enough to attain a smooth transition between the liquid and solid phase material at the melt-pool boundary. Typically, the element size is $\sim 3\%$ of melt-pool width or finer. The resulting solidification boundary may be tracked over time and sectioned to approximate melt-pool dimensions. This mesh refinement procedure was also used to predict the melt-pool dimensions and the structure and orientation of solidification grains for the NIST AM Benchmark competition where AMP² results achieved the second place [6].

The AMP² software tools gave options for approaching the unique process situations in the AFRL Challenge Statement 2. For the track pads, the macroscale analysis was used to characterize the heat buildup between layers (Fig. 4a). AMP² thermal simulation was used to directly predict melt-pool dimensions where temperature conditions were transient. In quasi-steady-state regions, the mesoscale thermal analysis was used to predict the in-layer heat buildup, and melt-pool thermal-CFD simulation was used to predict melt-pool dimensions. For the thin wall, only the melt-pool thermal-CFD simulation was used, since there is no build preheat (Fig. 4b).

Table 1 details which melt-pool model was used for each measurement plane. Note AFRL Challenge 2 required the dimensions and the standard deviation of the melt-pool cross-sectional measurement. The variability of the melt-pool cross section was attributed to the microscale nonuniformity of powder recoat, which was simulated using the Yade Discrete Element Method software [12]. The simulated value for the Coefficient of Variation (COV) for recoat powder relative density was

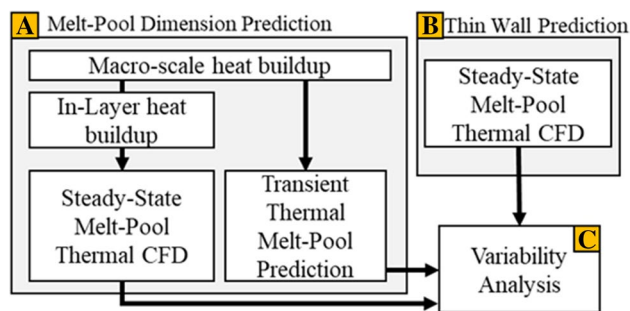


Fig. 4 Sequence of melt-pool analysis using AMP²

0.30, which was used estimate the attributes of variability for the melt-pool cross-sectional dimensions (Fig. 4c).

Results and Discussion

AMP² Prediction of Melt-Pool Dimensions

This section corresponds to Fig. 4a and discusses the macroscale thermal analysis using AMP², mesoscale thermal analysis using AMP², and microscale analysis using transient thermal and quasi-steady-state thermal-CFD models.

AMP² Macroscale and Mesoscale Heat Buildup Simulations

A macroscale simulation was performed for sample B26 to consider the influence of depositing 5 mm of material beneath the track deposits. The simulated temperature distributions for layers 5, 30, 60, 90, and 120 of challenge item B26 are shown in Fig. 5, where the macroscale model indicated that the entire substrate block would cool to ambient temperature before powder recoat. The top row of Fig. 5 shows the temperature distribution after all energy has been added (deposited) to the given layer, while the second row shows the temperature distribution after the cooling period (prior to recoat). As the blocks of material under all samples were similar, little to no heat buildup was expected for the blocks.

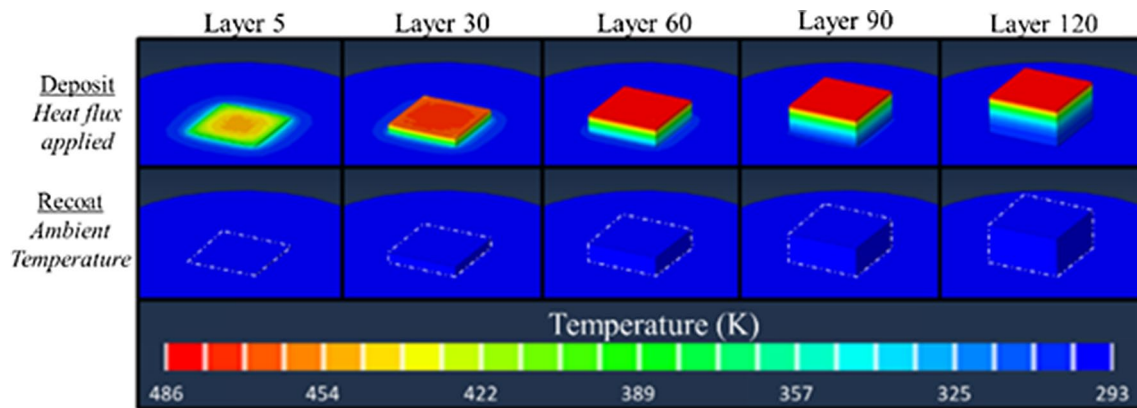


Fig. 5 Macroscale simulation results for challenge item B26

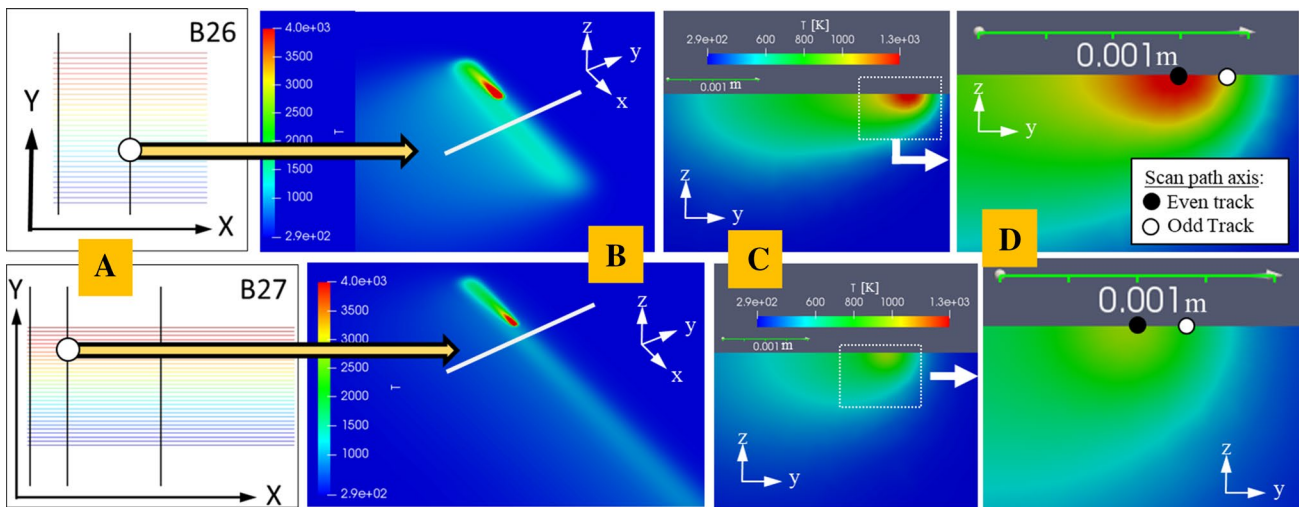


Fig. 6 Mesoscale temperature distribution for challenge items B26 (steady state) and B27 (quasi-steady state). **a** Scan paths for B26 and B27; **b** mesoscale simulation of odd tracks showing temperature of the melt pool immediately before crossing Measurement Plane 2 for

both B26 and B27; **c** cross section of temperature profile for conditions in image B for both B26 and B27; **d** enlarged view of image C to show scan path axes

The in-layer heat build was then simulated for samples B26 through B38, which were initialized at ambient temperature. Figure 6a shows Plane 2 for samples B26 and B27. This plane is the same distance from the edge of the tracks for each sample. Figure 6b shows an angled view of the temperature buildup, where Fig. 6c shows that the temperature in Plane 2, just prior to the laser passing over, is nearly 100 K larger for B26 than for B27. This difference results from the shorter track vector lengths used in sample B26. Figure 6d shows representative points where the temperature was measured to understand how heat buildup differed between even and odd tracks.

Figure 7a, b corresponds to samples B26 and B27, respectively. Of the 30 tracks deposited for items B26 and B27, only tracks 4 through 27 are displayed as the modeling challenge directed challengers to not take measurements for the first three and last three tracks of each challenge item. Each sample shows that the temperature arrives at a steady state

within the plane as more tracks are deposited, though this trend is specific to even and odd tracks. Sample B26 is consistently about 75 K hotter than the hottest temperatures in B27. Furthermore, the temperature can vary by up to 300 K between even and odd tracks for sample B27, i.e., using long track vectors can increase the thermal variability along a single track, which can change the resulting size and shape of the melt pool. When predicting melt-pool dimensions using a thermal-CFD simulation (Table 1), these temperature differences were considered by letting the temperature distribution (as in Fig. 6c) act as the initial conditions.

Steady-State and Transient Predictions of Melt-Pool Geometry

Figure 8 shows the representative simulation results from using scan path thermal and melt-pool thermal-CFD simulations to predict melt-pool dimensions. Figure 8a shows the

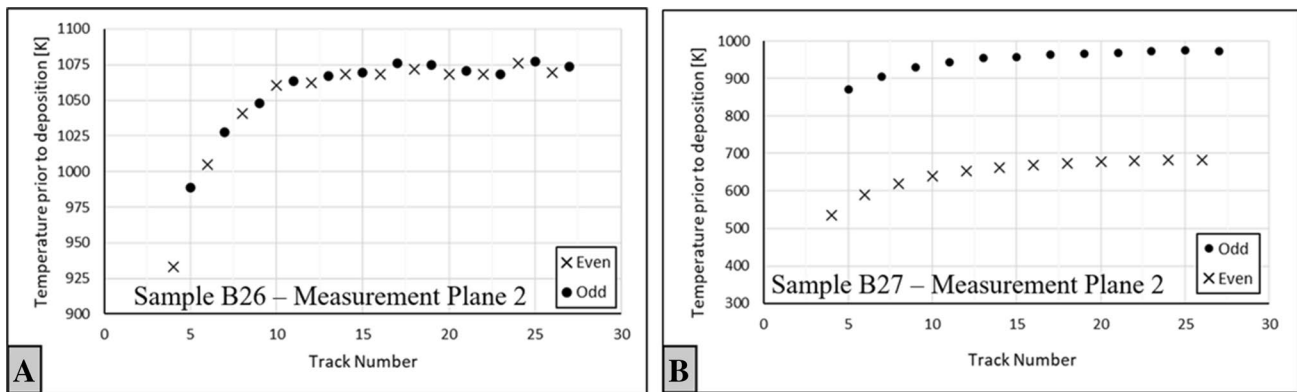


Fig. 7 Temperature along measurement plane 2 for challenge item a B26 showing steady-state temperatures and for b B27 showing quasi-steady-state temperatures. The temperature is taken on the plane immediately before the laser passes over it

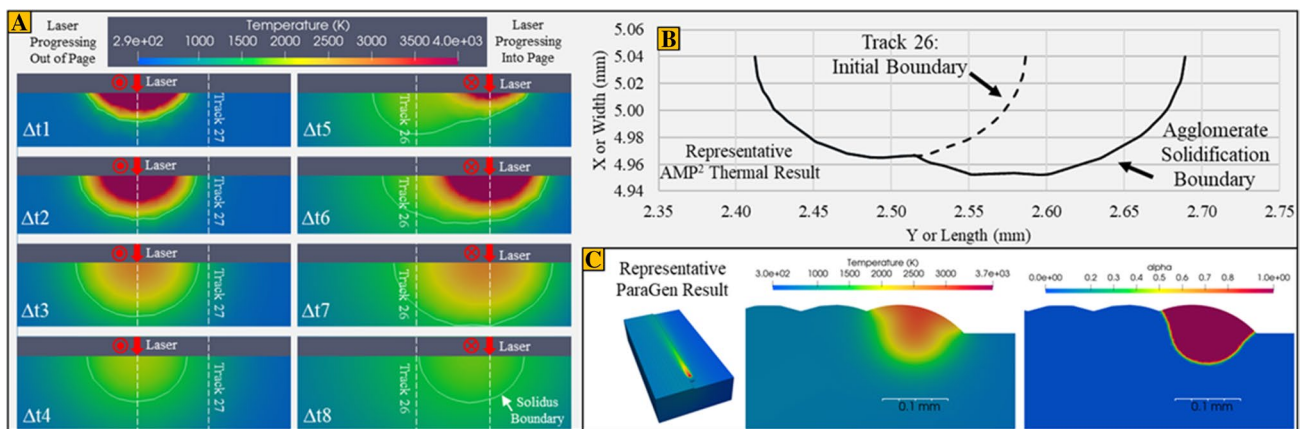


Fig. 8 Representative melt-pool predictions showing a transient AMP² thermal results for sample B27, plane tracks 26 and 27, where the melt-pool shape changes as the laser progresses in and out of the page, b the resulting AMP² thermal solidification boundary, where

the initial boundary is agglomerated into a larger boundary, and c representative melt-pool predictions from the thermal-CFD simulation for a different case, showing the steady-state temperature and solidification boundary

cross section of the melt pool across several time steps for sample B27, where the laser progresses out of and into the page. The liquidus boundary is represented as a white line. Note how track 26 does not finish solidifying by the time track 27 starts. The agglomerate boundary observed during metallography would therefore consist of the extents of both tracks, as shown in Fig. 8b. This cross section differs from the thermal-CFD simulation results, where only a single cross section is represented (Fig. 8c).

AFRL defined four measurements to evaluate each track [2]. Figure 9a shows these measurements defined by AFRL. The characteristics are defined as follows: (1) W_u is the distance along the Y -axis measured from the leftmost point of track n to the leftmost point of the next intersecting track, typically $n + 1$ (these two points may be at different Z values); (2) W_d is the distance along the Y -axis measured from the leftmost point of track n to the Y value that coincides with the lowest Z value on the track; (3) D_{tot} is the distance along the Z -axis measured from the lowest point of track n to the highest point of n (these points may not have the same Y value); (4) D_r is the distance along the Z -axis measured from the lowest point on track n to the Z value of the intersection of n and $n + 1$. For each measurement, three even tracks and three odd tracks were measured, and the mean and standard deviation for the measurements were reported and categorized as even or odd.

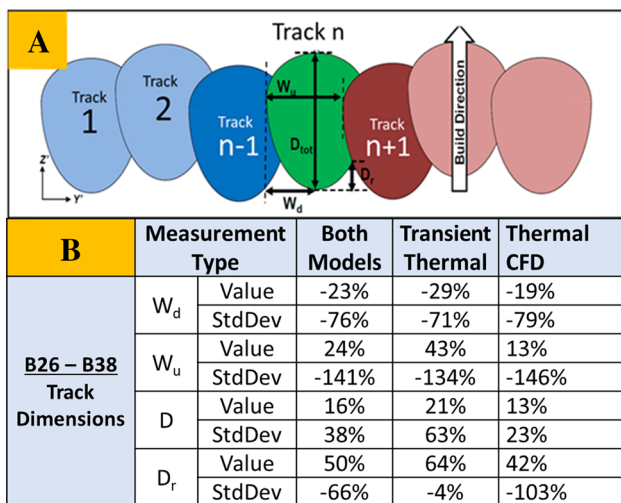


Fig. 9 a Melt-pool cross-sectional measurements given by AFRL where tracks appear quasi-steady. b Mean percent error between the predicted and measured track dimensions and standard deviations. The error of each column is calculated as: $\%Error = \frac{1}{n} \sum_1^n \frac{(Sim_n - Exp_n)}{Exp_n} * 100\%$, where Sim_n and Exp_n represent a single measurement point from the simulation and experimental measurements, respectively. For the “Thermal CFD” and “Transient Thermal” columns, n sums the error between Sim_n and Exp_n for individual simulation types. For the “Both Models” column, n sums the error between Sim_n and Exp_n across both simulation types

While melt-pool dimensions were directly measured from the steady-state simulations, the standard deviation was estimated using the local nonuniformity of powder recoat relative density. The percent error between the predicted and actual melt-pool dimensions is summarized Fig. 9b [2]. The actual and simulated N th-track dimensions are shown in Figs. 10 and 11, where the standard deviation is plotted as the error bars. Rather than denoting tracks as even and odd, tracks are denoted according to the scan direction along the X -axis (either negative or positive directions). In general, the thermal-CFD simulation predicted track dimensions better than the transient thermal simulation. The quasi-steady-state thermal-CFD simulation predicted D_{tot} , W_u , and W_d with a mean error of 13–19%, though the prediction of D_r was less accurate with a mean error of 50%. This larger difference for D_r can be expected since the exact value of D_r may vary more significantly than the other dimensions when transient phenomena occur. The standard deviation predictions could be improved by using a higher-order melt-pool model, though this is expected as the current predictions are obtained using a quasi-steady-state thermal-CFD solver. The predictions for W_d and D_{tot} are higher and lower, respectively, as compared to the experimental measurements. This is due to the approximation in the modeling of laser energy absorption as a uniform cylindrical heat source, which has a diameter equal to the laser spot size and extends down to the laser penetration depth. This uniform heat source approximation can result in overestimation of energy absorbed in the upper regions of the melt pool, leading to predicted widths that are wider and remelt depths that are shallower.

Microscale Thin Wall Simulation Results

This section corresponds to Fig. 4b. The quasi-steady-state thermal-CFD simulation was used to simulate track-on-track deposition for thin wall challenge items B21 and B25 (Fig. 12a, b). A typical microscale simulation requires an initial condition for temperature distribution that is generated by a mesoscale simulation. Such an initial condition is not necessary for the thin wall model because the tracks are deposited onto a substrate at ambient temperature. The initial geometry conditions for a track on layer k come from layer $k - 1$.

AFRL defined two measurements for the thin walls, which were the mean height of the wall (denoted as H in Fig. 12) relative to the substrate and mean cross-sectional area (indicated as A in Fig. 12) orthogonal to the scan vector (Fig. 12a, b). These measurements were taken for three measurement zones, depicted in Fig. 12c. Zones 1 and 3 are at the beginning and end of track deposition, respectively, and were expected to exhibit powder absorption which is more transient than in Zone 2. The quasi-steady-state thermal-CFD model was used to predict the steady-state

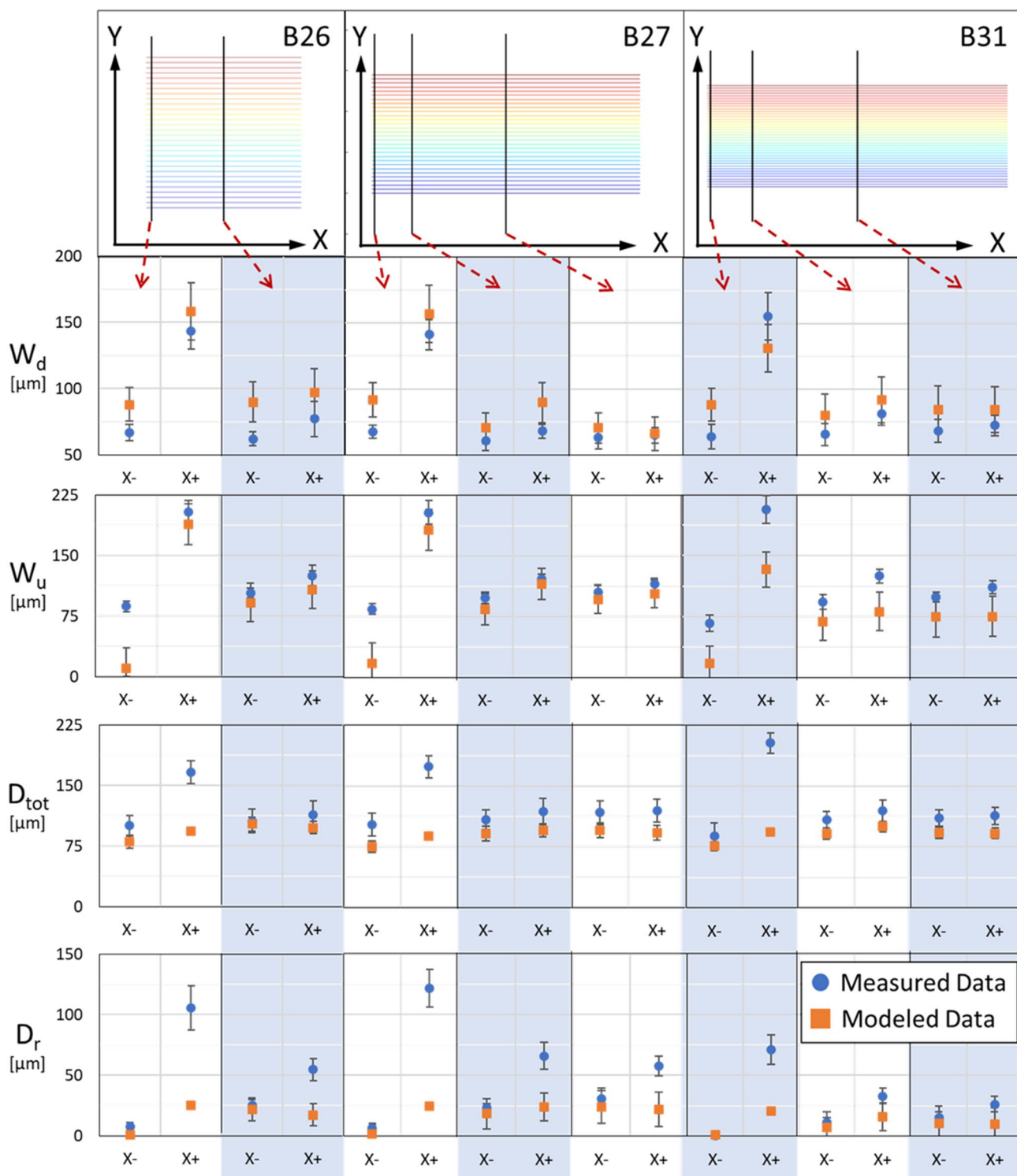


Fig. 10 Comparison between measured and modeled mean melt-pool dimensions for challenge items B26, B27, and B31. The error bars depict the measured and modeled standard deviation from the mean.

“X-” denotes that the scan is in the negative X direction and “X+” denotes that the scan is in the positive X direction

melt-pool dimensions for Zone 2. The remelt between tracks is higher for B21 than B25 due to higher input energy density. The track formation for various layers is similar for

most layers, except B21 layer 5 where the remelt depth is marginally higher. Such difference in track cross section can be minimized by using a tighter convergence tolerance in the

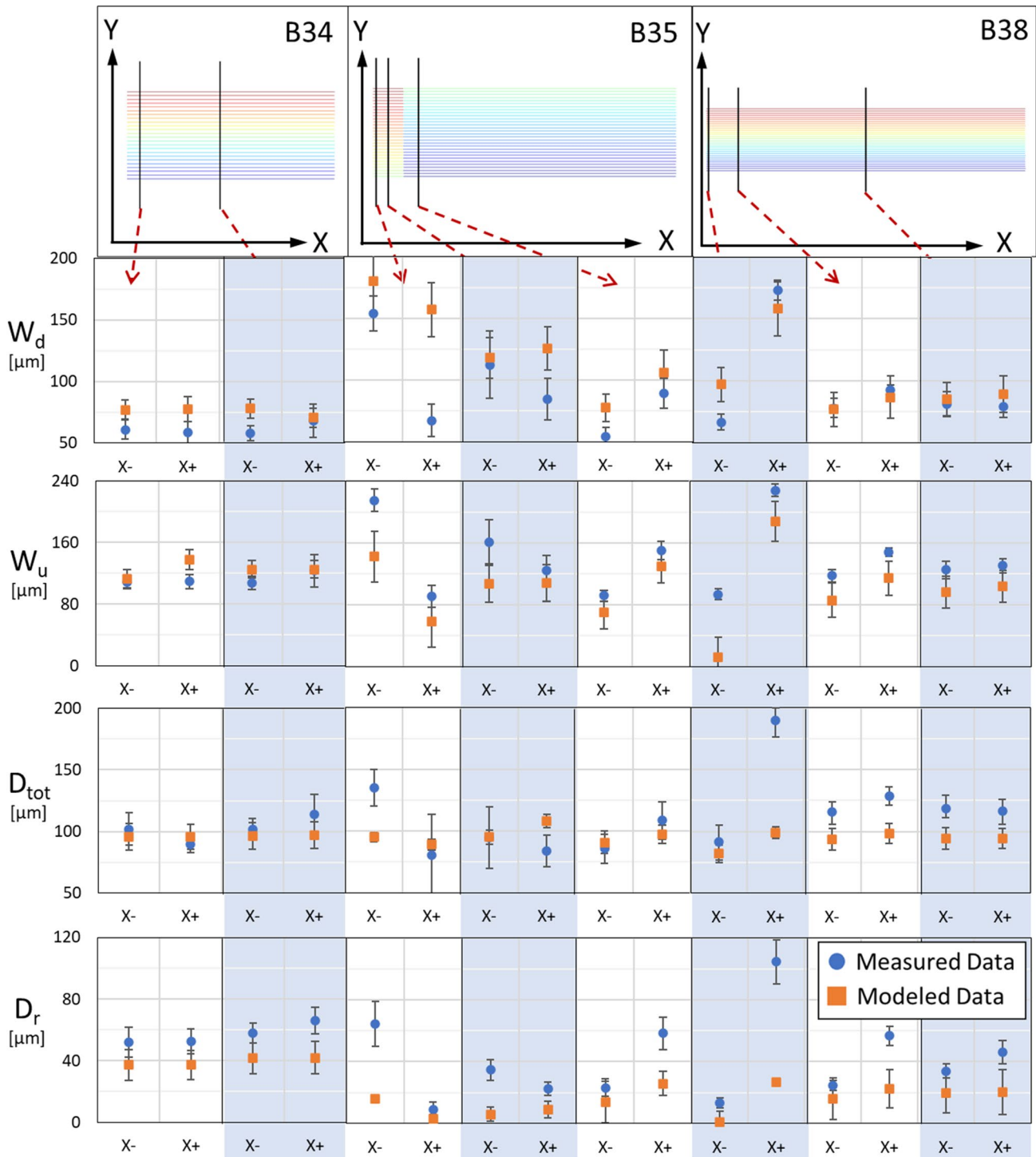


Fig. 11 Comparison between measured and modeled mean melt-pool dimensions for challenge items B34, B35, and B38. The error bars depict the measured and modeled standard deviation from the mean.

“X-” denotes that the scan is in the negative X direction and “X+” denotes that the scan is in the positive X direction

numerical iterations. The build height for Zones 1 and 3 was estimated by considering the changes in the PDZ and laser power at the start and end of track. The PDZ for track start-up with laser power ON (Zone 1) assumed the formation of

PDZ on the back side of the melt pool. The track end with laser power OFF (Zone 3) assumed an abrupt end to PDZ formation ahead of the melt pool. The melt-pool predictions and corresponding error as compared to the measurements

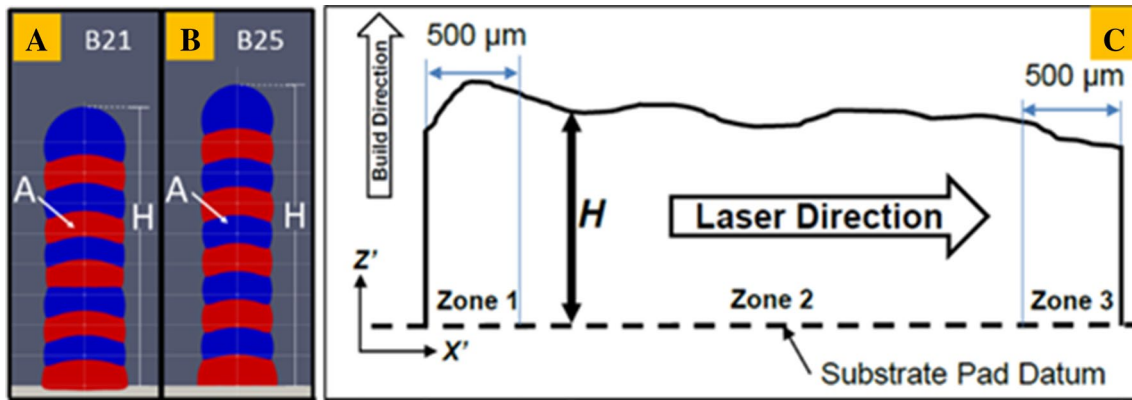


Fig. 12 Front view of thin wall with measurement definitions for challenge items **a** B21 and **b** B25. The depicted track cross sections were generated by the microscale model. The faint horizontal lines indicate powder bed heights for each layer, and the faint vertical lines

indicate the center of the thin wall. **c** Side view of thin wall with height measurement definition as well as measurement zone definitions. This figure was furnished by the AFRL

are shown in Fig. 13. The mean standard deviations are shown by the error bars. The percent error of H and A is 23% and 36%, respectively. The trends between the predicted and measured values are fairly consistent.

Conclusions

This article presents the results for the 2nd Challenge in the MID3AS AM Challenge. The predictions for N th-track cross-sectional dimensions were reported for six rectangular pads and two thin walls. The AM process parameters and pad dimensions were varied to create a variety of combinations for thermal and geometry conditions for the formation of the N th track. The pad geometry after the $(N - 1)$ st track was used as the substrate for the N th-track simulation. The predictions include track formation under quasi-steady-state and transient conditions, which were predicted using two types of melt-pool simulations: a thermal-CFD simulation and a transient thermal simulation. The thermal-CFD simulation solved incompressible Navier–Stokes equations and performed thermal-fluid geometry iterations to converge upon the quasi-steady-state, melt-pool cross-sectional geometry. The transient thermal simulation performed incremental thermal simulations within individual tracks in the scan path to account

for the merging of the melt pools due to zigzag of scan velocity in the scan path. The statistics of track cross-sectional dimensions was estimated by accounting for the variability of additive mass per unit length of the track caused by the local nonuniformity of powder recoat. The effect of residual heat due to the deposition of preceding layers was small, but the effect of residual heat due to the deposition of the first $(N - 1)$ tracks was significant, the character of which is a function of permutations of values for pad dimensions and its subdivision, power, speed, hatch spacing, layer thickness and total number of tracks (Fig. 1). For example, Fig. 7 shows how the residual heat for odd and even tracks at measurement plane 2 is different for samples B26 and B27, which are same except for their 3 mm and 10 mm pad length, respectively. As a result, the measurement plane 2 is at the center of B26 and is on the left side of B27, which means that the time taken to return to measurement plane 2 is significantly higher for even tracks as compared to odd tracks. The temperature distribution due to residual heat was used as initial conditions for the melt-pool simulations. The simulations were performed using the AMP² software and based on the accuracy of predictions with the experimental data. AO achieved third place for the 2nd Challenge in the MID3AS AM Challenge. In general, the simulation of transient melt-pool formation and track-on-track deposits was more complex and these conditions can be further explored in future competitions and validation efforts.

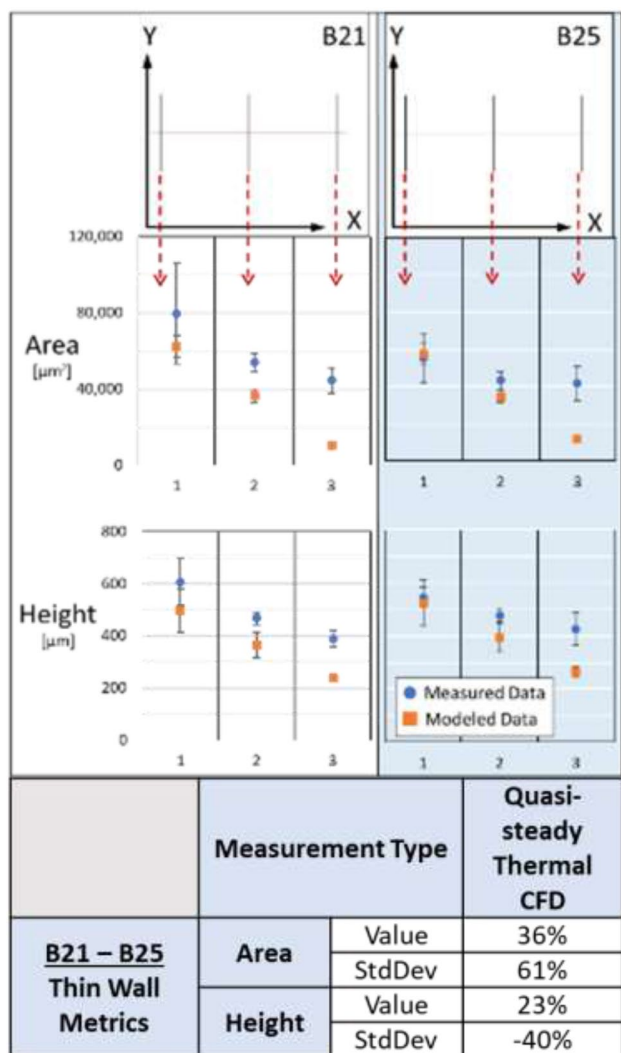


Fig. 13 Comparison between measured and modeled mean thin wall dimensions for challenge items B21 and B25. The error bars depict the measured and modeled standard deviation from the mean. The measurement zone is indicated by the number on the X-axis. The mean percent error across all measurements is given in the table

Acknowledgements Applied Optimization, Inc. (AO) is grateful for the opportunity to compete in the Air Force Research Laboratory (AFRL) Materials Inform Data-Driven Design for Additive Structures (MID3AS) AM (Additive Manufacturing) Challenge and acknowledges the efforts by Dr. Marie Cox and Dr. Edwin Schwalbach in the organization and follow-up for the MID3AS AM Challenge and the effort to ensure the efficacy of experimental data. AO also is grateful for

the support we have received from the Naval Air Systems Command (NAVAIR), National Aeronautics and Space Administration (NASA), and Office of Naval Research (ONR) SBIR programs and their respective technical monitors, Dr. William Frazier (Retired), Dr. Madan Kirtur, Nam Phan, and Mike Kasprzak (NAVAIR), Dr. Kevin Wheeler (NASA), and Dr. David Shifler (ONR), who supported the development of various algorithms for Additive Manufacturing (AM) process simulations, which are integrated into the AM Parameter Predictor (AMP²) software suite. AO is also grateful to Benjamin Schultheis for the early simulations and reports prepared for the MID3AS AM Challenge.

Declarations

Conflict of interest The Additive Manufacturing Parameter Predictor (AMP²) software used to simulate the ICME process and optimize parameters was developed at Applied Optimization, Inc., who produced this article.

References

- Groeber M, Schwalbach E, Musinski W, Shade P, Donegan S, Uchic M, Sparkman D, Turner T, Miller J (2018) A preview of the US air force research laboratory additive manufacturing modeling challenge series. *JOM* 70(4):441–444
- Air Force Research Laboratory, Materials Inform Data-Driven Additive Structures. <https://github.com/materials-data-facility/MID3AS-AM-Challenge>. Accessed 07 Mar 2021
- Cox ME, Schwalbach EJ, Blaiszik BJ, Groeber MA (2021) AFRL additive manufacturing modeling challenge series overview. *Integr Mater Manuf Innov* 10(2):125–128
- Schwalbach EJ, Chapman MG, Groeber MA (2021) AFRL additive manufacturing modeling series: challenge 2—microscale process to structure data description. *Integr Mater Manuf Innov*. <https://doi.org/10.1007/s40192-021-00220-9>
- Carnegie Mellon University (2017) Carnegie Mellon University and Applied Optimization, Inc. selected for awards under the Modelling Challenge for AM. https://www.cmu.edu/engineering/materials/news_and_events/news/archive/2017/march/america-makes-pistorius-rollett.pdf
- Robichaud J, Vincent T, Schultheis B, Chaudhary A (2019) Integrated computational materials engineering to predict melt-pool dimensions and 3D grain structures for selective laser melting of Inconel 625. *Integr Mater Manuf Innov* 8(3):305–317
- Wormald S, Clingenpeel J, Chaudhary A, Kasprzak M, Phan N (2020) Determination of melt-pool cross-section objective metrics to enable the optimization of laser powder bed fusion process parameters for structural parts: core exposure defect reduction. Submitted to NAVAIR for Public Release Authorization, December 2020
- Wormald S, Clingenpeel J, Chaudhary A, Kasprzak M, Phan N (2020) Determination of melt-pool cross-section objective metrics to enable the optimization of laser powder bed fusion process parameters for structural parts: contour exposure melt pool

- objective. Submitted to NAVAIR for Public Release Authorization, December 2020
9. Wormald S, Clingenpeel J, Chaudhary A, Kasprzak M, Phan N (2020) Utilization of melt-pool cross-section objective metrics to enable the optimization of laser powder bed fusion process parameters for structural parts: optimization of core-to-contour fusion. Submitted to NAVAIR for Public Release Authorization, December 2020
 10. Wormald S, Clingenpeel J, Chaudhary A, Kasprzak M, Phan N (2020) Utilization of melt-pool cross-section objective metrics to enable the optimization of laser powder bed fusion process parameters for structural parts: site-specific quality control. Submitted to NAVAIR for Public Release Authorization, December 2020
 11. Applied Optimization, Inc. Rapid, low cost, high-quality component qualification using multi-scale, multi-physics analytical tool-set for the optimization of metal additive manufacturing process parameters. Final report, NAVAIR SBIR Topic N162-083 Phase II, Contract: N68335-19-C-0299
 12. Yade (2009) Open source discrete element method. <https://yade-dem.org/doc/>. Accessed 07 Mar 2021

Publisher's Note Springer Nature remains neutral with regard to jurisdictional claims in published maps and institutional affiliations.